

# Lab on a Chip

Accepted Manuscript



This is an *Accepted Manuscript*, which has been through the Royal Society of Chemistry peer review process and has been accepted for publication.

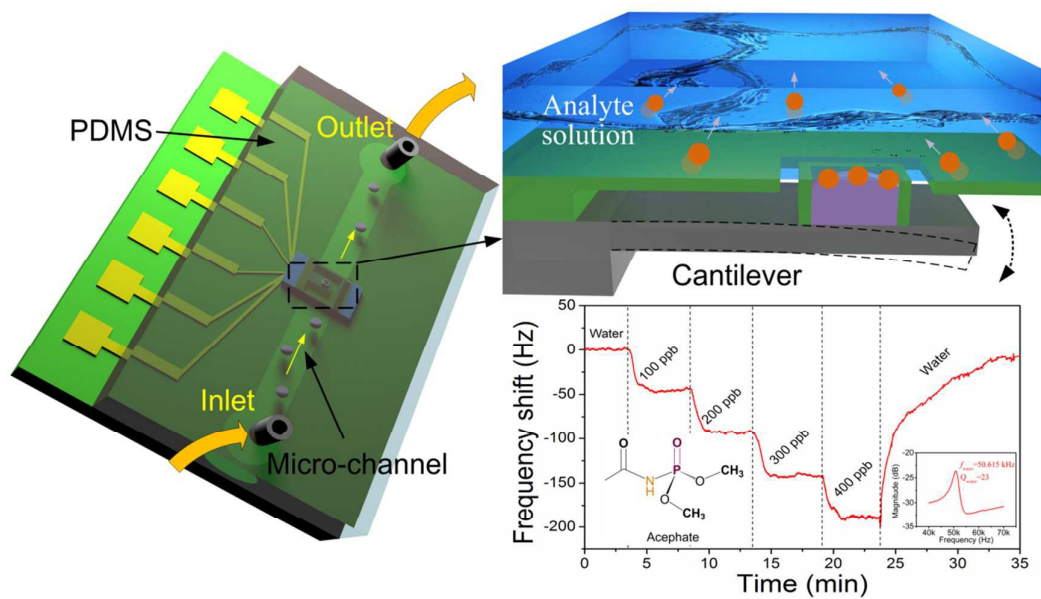
*Accepted Manuscripts* are published online shortly after acceptance, before technical editing, formatting and proof reading. Using this free service, authors can make their results available to the community, in citable form, before we publish the edited article. We will replace this *Accepted Manuscript* with the edited and formatted *Advance Article* as soon as it is available.

You can find more information about *Accepted Manuscripts* in the [Information for Authors](#).

Please note that technical editing may introduce minor changes to the text and/or graphics, which may alter content. The journal's standard [Terms & Conditions](#) and the [Ethical guidelines](#) still apply. In no event shall the Royal Society of Chemistry be held responsible for any errors or omissions in this *Accepted Manuscript* or any consequences arising from the use of any information it contains.

**Graphical Abstract**

A  $\mu$ -'diving suit' technology is developed to achieve long-time stable resonance of micro-cantilever sensors in solution for real-time bio/chemical detection.





## Lab on a Chip

### PAPER

## $\mu$ -‘diving suit’ for liquid-phase high- $Q$ resonant detection

Haitao Yu, Ying Chen, Pengcheng Xu, Tiegang Xu, Yuyang Bao and Xinxin Li\*

Received 00th January 20xx, \

Accepted 00th January 20xx

DOI: 10.1039/x0xx00000x

[www.rsc.org/](http://www.rsc.org/)

Resonant cantilever sensor is, for the first time, dressed in a water-proof ‘diving suit’ for real-time bio/chemical detection in liquid. The  $\mu$ -‘diving suit’ technology can effectively avoid not only unsustainable resonance due to heavy liquid-damping, but also inevitable nonspecific adsorption on the cantilever body. Such a novel technology ensures long-time high- $Q$  resonance of the cantilever in solution environment for real-time trace-concentration bio/chemical detection and analysis. After the formation of integrated resonant micro-cantilever, patterned photoresist and hydrophobic parylene thin-film are sequentially formed on top of the cantilever as sacrificial layer and the water-proof coat, respectively. After sacrificial-layer release, air gap is formed between the parylene coat and the cantilever to protect the resonant cantilever from heavy liquid damping effect. Only a small sensing-pool area, located at the cantilever free-end and locally coated with specific sensing-material, is exposed to the liquid analyte for gravimetric detection. The specifically adsorbed analyte mass can be real-time detected by recording the frequency-shift signal. In order to secure vibration movement of the cantilever and, simultaneously, reject liquid leakage from the sensing-pool region, a hydrophobic parylene made narrow slit structure is designed surrounding the sensing-pool. The anti-leakage effect of the narrow slit and damping limited resonance  $Q$ -factor are modelled and optimally designed. Integrated with electro-thermal resonance exciting and piezoresistive frequency readout, the cantilever is embedded in a micro-fluidic chip to form a lab-chip micro-system for liquid-phase bio/chemical detection. Experimental results show the  $Q$ -factor of 23 in water and longer than 20 hours liquid-phase continuously working time. Loaded with two kinds of sensing-materials at the sensing-pools, two types of sensing chips successfully realize real-time liquid-phase detection to ppb-level organophosphorous pesticide of acephate and *E.coli* DH5 $\alpha$  in PBS, respectively. The proposed method fundamentally solves the long-standing problem of unable to well operate resonant micro-sensor in liquid.

### Introduction

Lab-on-a-chip (LOC) has been expected to become an evolutionary tool for highly functional, compact and rapid instruments for bio/chemical analysis, recognition, synthesis and related sciences and technologies.<sup>1-3</sup> Among the LOC techniques, rapid sensing LOCs<sup>4-6</sup> for real-time detection of trace-level bio/chemical analytes, e.g., residual pesticides in soil or harmful pathogens in water, are highly demanded in the application fields such as food safety,<sup>7,8</sup> environment protection<sup>9</sup> and human health<sup>10</sup>. Among the recently developed bio/chemical sensors with MEMS (micro-electro-mechanical systems) techniques, resonant micro-cantilevers<sup>11</sup> have been highly expected in various on-the-spot trace-level detection/analysis microsystems due to ultra-high sensitivity, miniaturized device size, integration compatibility with standard CMOS processes and low fabrication-cost, etc.<sup>12-15</sup> With functionalized sensing-probe material coated at the free-end, the resonant micro-cantilever is enabled for label-free quantitative measurement of specifically adsorbed mass,

thereby building a micro-gravimetric platform technology for various on-site LOC bio/chemical applications.<sup>16-19</sup>

The working principle of resonant micro-cantilevers lies in frequency-shift ( $\Delta f$ ) induced by adsorbed analyte mass ( $\Delta m$ ).<sup>20,21</sup> As long as  $\Delta m$  is much smaller than the cantilever mass  $m$ ,  $\Delta f$  is proportional to  $\Delta m$ . The limit of detection (LOD) is determined by minimum detectable  $\Delta m$ , which is generally proportional to the reciprocal of  $Q$ -factor of the cantilever. When the micro-resonator is worked in air for gas sensing, the  $Q$ -factor is dominated by the slight air-damping and, in general, is high enough to achieve a pico-gram level LOD. Thus, it is not very difficult to use the resonant micro-cantilever sensors in air. Unfortunately, the flexural-bending resonant devices are hardly operated in solution for real-time bio/chemical detection, due to the significantly decreased  $Q$ -factor caused by the severe viscous drag effect of liquid.<sup>22,23</sup> To fulfil the demand of bio/chemical detection in liquid, efforts were ever made to reduce the liquid drag effect. One approach tried to operate the resonant micro-cantilever working in higher resonance modes such as torsional one or in-plane swing one.<sup>24,25</sup> However, the resonant frequency of higher mode will be much higher than that of the fundamental bending mode. The much higher mechanical stiffness makes the cantilever hard to be excited into higher-mode resonating. An alternative attempt is to embed micro-fluidic channel into the cantilever

State Key Lab of Transducer Technology, Shanghai Institute of Microsystem and Information Technology, Chinese Academy of Sciences, 865 Changning Road, Shanghai 200050, China.  
E-mail: xxli@mail.sim.ac.cn; Fax: +86 21 62513510; Tel: +86 21 62131794

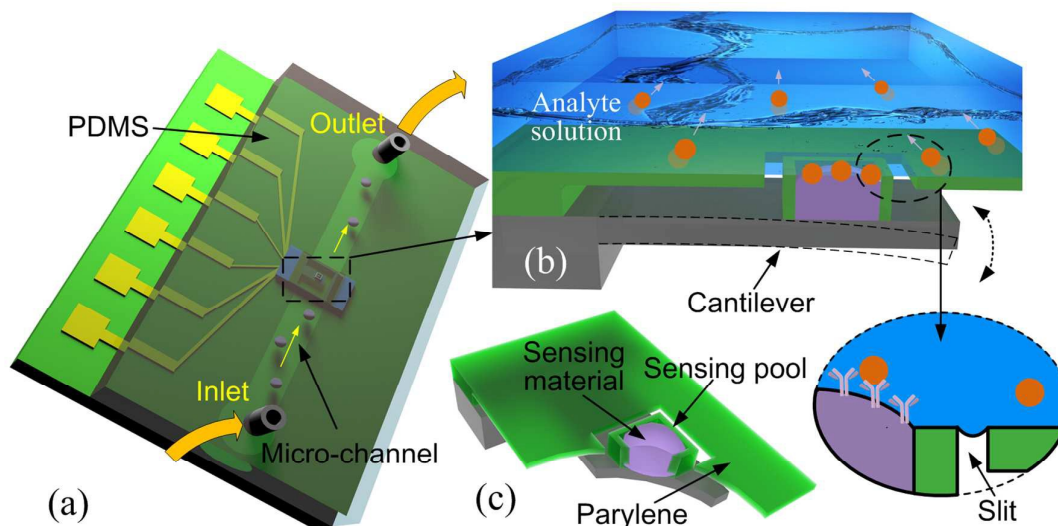


Fig. 1 (a) Schematic of the bio/chemical sensing LOC system, in which a resonant-cantilever sensor is embedded. (b) and (c) Cross-sectional schematic and partly cut view both showing the  $\mu$ -'diving suit' structure for the liquid-phase operated resonant-cantilever. Main body of the resonant-cantilever is isolated from liquid analyte by a parylene-film made  $\mu$ -'diving suit', while only the sensing-pool area contacts the liquid. The close-up schematic of (b) shows the solution-proof mechanism of the narrow slit for free vibration of the cantilever. The sidewalls of the narrow slit are made of hydrophobic parylene for preventing from solution leakage.

to form a suspended microchannel resonator (SMR). The SMR sensors were used to weigh nanoparticles, viruses and small proteins in water.<sup>26</sup> However, the resonant SMR is not suited for detection of bigger sized bio-substance like cells, due to the limited microchannel depth. The thicker the channel, the thicker and the stiffer the cantilever is. Too rigid a cantilever is difficult to be excited into sufficient vibration for resonance measurement. In addition, optical detection like that in an AFM (atomic force microscopy) is used for the SMR. The sensing system will be expensive and hard to handle. The both weaknesses of SMR limit its applications in rapid on-the-spot bio-sensing. J. Park and his co-workers presented a critical operation method where the micro-cantilever resonates at the interface of air and liquid.<sup>27</sup> By this means the  $Q$ -factor at resonance is improved to 15, which is 50% higher than the same cantilever resonating in liquid. This is a nice idea to improve resonance by reducing the contact area with liquid. However, one whole side of the cantilever facing to the liquid is still quite large and the benefit for  $Q$ -factor is limited.

It is worthy pointing out that, all the afore-mentioned efforts have a common shortcoming. Having a large contacting area with liquid, such resonant cantilever generally suffer the cross influence from nonspecific bio-adsorption induced false frequency-shift signal.

In this paper, we propose a new liquid-phase gravimetric detection method, where a gas/liquid separated resonant micro-sensor with high  $Q$ -factor in solution is developed for real-time bio/chemical sensing. As is schematically demonstrated in Fig. 1, a water-proof  $\mu$ -'diving suit' is fabricated to cover the cantilever resonator. With a narrow hydrophobic slit structure specifically designed to secure both anti-leakage and free vibration of the cantilever, the bio/chemical sensing-region at the cantilever free-end is exposed to the targeted analyte solution while the other parts

of the sensor are remained in air to keep long-time high- $Q$  resonance. This novel technique can drastically decrease the influence of the liquid media damping effect, thereby achieving high- $Q$  resonant sensing for accurately detecting trace-level bio/chemical substance in solution. Moreover, the technique features following advantages: (1) protecting the cantilever structure from nonspecific adsorption for reliable detection; (2) being suitable for and extendable to various liquid-sensing devices with various structural geometries; (3) the narrow hydrophobic slit structure can be flexibly design for variously shaped solution-contact area; (4) the  $\mu$ -'diving suit' can be low-cost batch fabricated in wafer-level. At last, such resonant structures can be integrated in various micro-fluidic lab-chip micro-systems, where the targeted analyte solution, elution solution and liquid buffers can sequentially flow in and out, for real-time bio/chemical analysis in liquid. This lab-chip scheme can be referred to Fig. 1a.

## Design and modelling

### Water-proof mechanism of the $\mu$ -'diving suit'

The  $\mu$ -'diving suit' configuration design is schematically shown in Figs. 1b and 1c. A shell is constructed above the resonating cantilever by using hydrophobic parylene film. An air gap-distance is formed in between by sacrificial-layer release for free resonance of the cantilever in air. When the device is merged into liquid, the top side of the cantilever can be protected by the water-proof parylene film from contact with liquid, with an exception that the small sensing-material area, namely sensing-pool, at the cantilever free-end is exposed to the analyte solution for specific bio/chemical interaction. The slit constructed between the hydrophobic parylene outer-wall of the sensing-pool and the inner-edge of the parylene

opening can secure no liquid leakage, even when the sensing-pool is vibrated together with the cantilever. Even if the water vapour goes into the structural inside after the device works in a solution for a long period of time, the humidity can be captured by a small piece of absorbing agent pre-placed from the opened backside of the cantilever. A polydimethylsiloxane (PDMS) cover is constructed to embed the water-proof sensing cantilever to form a micro-chip, where micro-channels are connected to allow the analyte solution flow through. As is pointed out in Ref. 28, the mass sensitivity at different location along the cantilever length is different. From the clamped-end to the free-end, the mass sensitivity increases from zero to the maximum value. Thus, locating the sensing-pool near the cantilever free-end helps to enhance the sensor response from the minimally exposed sensing area to liquid, meanwhile, gets very little loss of  $Q$ -factor compared with immobilizing the sensing material on the whole cantilever surface. Such a sensing-pool location is also helpful for eliminating stiffness change of the cantilever that counteracts the mass change signal. It is known that the stiffness changing effect of the cantilever is strong when the sensing location is near the cantilever clamp-end but negligible near the free-end.<sup>13</sup>

#### Hydrophobic-slit induced sustention of vibration in liquid

The narrow slit constructed between the walls of the sensing-pool and the opening edge of the water-proof  $\mu$ -'diving suit' plays an important role to reject liquid leakage. Since the plasma etching to the parylene film is an isotropic process, the shape at the etched sidewalls is rostriform instead of rectangular, as is schematically shown in Fig. 2. Thus the angles at the etched corners are  $\delta_1 \geq 135^\circ$  and  $\delta_2 \leq 45^\circ$ , respectively. There are two stable states, at either of which the liquid can be stayed. One is called Cassie–Baxter (C–B) state<sup>29</sup> and shown in Fig. 2b. Another is Wenzel state<sup>30</sup> and shown in Fig. 2c. At either of the two states, the supporting air pressure  $P_0$  should be balanced with the imposed liquid pressure  $P_1$ . In which state the liquid is pinned is determined by the apparent liquid contact-angle (CA) with the edge,  $\theta_{\text{pin}}$ . Gibbs inequalities are used to calculate the pinned range, i.e. the maximum and the minimum pinning contact-angles, with following expression of<sup>31</sup>

$$\theta_Y \equiv \theta_{\min} \leq \theta_{\text{pin}} \leq \theta_{\max} \equiv \pi - \delta_1 \text{ or } 2 + \theta_Y \quad (1)$$

where  $\theta_Y$  is the intrinsic CA (obtained by the liquid-drop CA test, shown in Fig. 2a),  $\theta_{\min}$  and  $\theta_{\max}$  are the minimum and the maximum pinning CAs with the edge, respectively. Outside the range from  $\theta_{\min}$  to  $\theta_{\max}$ , the liquid cannot be pinned and the

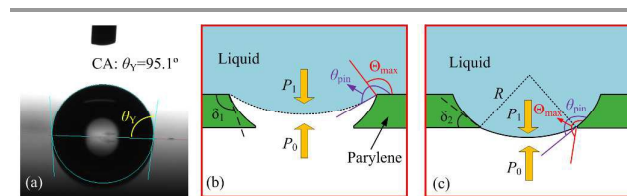


Fig. 2 (a) Tested 95.1° water-drop contact-angle (CA) for the hydrophobic parylene film. (b) Illustration of C-B state: water is pinned on upper corners of the hydrophobic slit. (c) Illustration of Wenzel state: water is pinned on lower corners of the hydrophobic slit.

interface will have to move.

Firstly we suppose that the liquid (herein water) is pinned on the upper side of the slit (i.e., C–B state shown in Fig. 2b), we calculate  $\theta_{\max} \leq 140.1^\circ$  and  $\theta_{\min} = 95.1^\circ$  by using Eq. (1), i.e. the pinned range should be from  $95.1^\circ$  to  $140.1^\circ$ . Practically however, in this case the apparent CA of  $\theta_{\text{pin}}$  must be larger than  $180^\circ$  that is outside the pinned range. Hence the C–B state cannot be maintained and the state will be turned into the Wenzel state of Fig. 2c. In this state, we calculate  $230.1^\circ \leq \theta_{\max} < 275.1^\circ$  and  $\theta_{\min} = 95.1^\circ$ , i.e., the pinned range should be from  $95.1^\circ$  to a larger angle between  $230.1^\circ$  and  $275.1^\circ$ . By appropriately setting the pressure difference of  $\Delta P = P_1 - P_0$ , the  $\theta_{\text{pin}}$  value can be easily controlled within this very wide range. According to this pinned range, we can inversely calculate the maximum pressure difference  $\Delta P$  by using Young-Laplace equation of

$$\Delta P = P_1 - P_0 = 2\gamma/R \quad (2)$$

while  $\gamma$  is liquid surface tension and  $R$  is curvature radius of the interface shape. If the width at the bottom of the slit is denoted as  $t$ , we have  $t = 2R\cos(\theta_{\text{pin}} + \delta_2 - 180^\circ)$ , and the pressure difference can be deduced as

$$\Delta P = 2\gamma\cos(\theta_{\text{pin}} + \delta_2 - 180^\circ)/t \quad (3)$$

by substituting  $R$  with  $t$ . From Eq. (3), we can work out the maximum pressure difference as

$$\Delta P_{\max} = 2\gamma/t \quad (4)$$

when  $\theta_{\text{pin}} = 180^\circ - \delta_2$ . It can be seen from Eq. (4) that, the smaller the slit width  $t$ , the larger the balanced pressure at the interface. Besides, the calculated  $\Delta P_{\max}$  indicates upper limit of the pressure difference used in the micro-fluidic system. In this study, the slit is designed as narrow as about 10 microns. Since the liquid surface tension of water is 0.072 N/m at room temperature, we work out the maximum usable  $\Delta P$  at the interface as about 14.4 kPa. The  $\gamma$  values of most chemical or biological solutions are larger than that of water, which means that the practically usable  $\Delta P_{\max}$  in bio/chemical sensing experiment can be larger than 14.4 kPa. During experimental bio/chemical detection, lower pressure difference than this value is kept to avoid liquid leakage.

#### Damping effect and resonance $Q$ -factor

It can be seen in Fig. 1 that, there is an air gap between the silicon resonant cantilever and the parylene film of the  $\mu$ -'diving suit' to form a space for free vibration of the cantilever. This gap-size should be well designed, as it strongly influences the damping effect, thereby dominantly influencing resonating  $Q$ -factor of the sensing cantilever. Firstly we consider the situation of working in air, where air damping effect on the cantilever resonance should be mainly considered. For a micro-cantilever vibrating in flexural bending mode and its geometric length, width and thickness are denoted as  $L$ ,  $W$  and  $T$ , respectively, the air damping can be calculated. According to the gap-size,  $G$ , the damping effect can be dominated by either squeeze-film air damping when  $G \ll W/2$  or drag-force damping when  $G \gg W$ .<sup>32</sup> In our study the width of the cantilever is designed as 100  $\mu\text{m}$  and the gap-size of less than 15  $\mu\text{m}$  is formed by release of sacrificial photoresist layer. It is

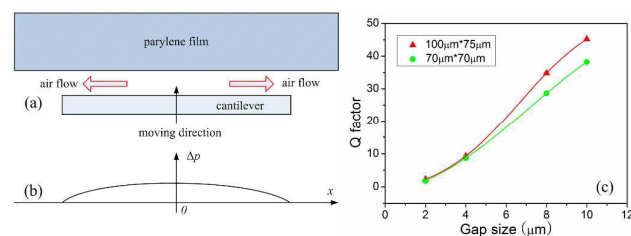


Fig. 3 Schematic squeeze-film air damping effect between the air gap is shown in (a) and the inside pressure distribution is illustrated in (b). (c) Finite-element simulation results for in-air  $Q$ -factor of the cantilever with varied gap-sizes and opening-sizes of the  $\mu$ -'diving suit' for contacting with liquid analyte.

apparent that squeeze-film air damping plays the dominant role in restriction of the resonance  $Q$ -factor. Figs. 3a and 3b show the schematic of squeeze-film air damping. When the resonant cantilever moves towards or away from the parylene plane, the built-up air pressure inside the air gap induces viscous damping in the confined spaces, which is known as squeeze-film damping.<sup>33,34</sup>

Since the displacements at different locations of the resonant cantilever are non-uniform, there is no close-form solution for solving the damping-force of cantilever vibration. Therefore, two simplified assumptions are introduced to obtain approximate solution. Firstly, we suppose that the movement of the cantilever keeps in parallel with the parylene plane and the oscillation is along the normal direction. Secondly, the relatively small opening area on the parylene film (i.e. at the sensing region) is ignored. Derived from Reynolds' Equation,<sup>35</sup> the coefficient of damping force can be expressed as

$$c = \frac{\mu L W^3}{G^3} \beta \left( \frac{W}{L} \right) \quad (5)$$

Herein  $\mu$  represents viscosity coefficient of air. At room temperature of 273 K,  $\mu = 17.2 \times 10^{-6}$  Pa·sec.  $\beta$  is a factor which depends on the width/length ratio  $W/L$  of the cantilever.<sup>36</sup> For our cantilever,  $W = 100 \mu\text{m}$  and  $L = 200 \mu\text{m}$ . Therefore  $\beta = 0.71$ . In the proposed resonant-cantilever detection system, air damping is the main energy-dissipation mechanism. Hence the  $Q$ -factor can be calculated with  $Q = m\omega/c$ , where  $\omega$  is the circular frequency of the resonant cantilever and  $m$  is the mass of the silicon cantilever. Finally we have

$$Q = \frac{\rho T G^3 \omega}{\beta (W/L) \mu W^2} \quad (6)$$

where  $\rho$  is density of silicon cantilever. Theoretically, Eq. (6) indicates that the larger the gap-size, the higher the  $Q$ -factor. However, the achievable gap-size is also governed by fabrication process.

The size of the opening on the parylene film for the sensing-pool is another important parameter which also influences the  $Q$ -factor of the resonant cantilever. Obviously, increasing the opening area will decrease the fraction of squeeze-film air damping and bring about higher resonant  $Q$ -factor in air. For the complex model, we used finite-elements software of COMSOL to simulate the air-damping confined  $Q$ -factor with respect to gap-size and opening area, with the results shown in Fig. 3c.

As for the cantilevers working in liquid, the parylene-film covered part of the cantilever still resonates in air, while the

sensing-pool at the opening area will become to suffer the heavier liquid damping. Therefore, the opening area of the parylene-film should be comprehensively considered for both adsorbing adequate bio/chemical mass and high enough resonating  $Q$ -factor. Detailed analysis about a cantilever operating resonating in liquid can be found in Ref. 37.

## Experimental

### Fabrication process of the sensing micro-chip

The micro-cantilevers are with electro-thermal resonance exciting heater and piezoresistors for sensing-signal readout integrated. The cantilever dimensions are  $200 \mu\text{m} \times 100 \mu\text{m} \times 3 \mu\text{m}$ . The gap-size  $G$  between the parylene-film and the cantilever top surface is varied as  $8 \mu\text{m}$  and  $12 \mu\text{m}$ , respectively, to examine the effect of the squeeze-film air damping on  $Q$ -factor. The area of the opening on the parylene-film (for bio/chemical sensing) is designed with different sizes of  $70 \mu\text{m} \times 70 \mu\text{m}$  and  $100 \mu\text{m} \times 75 \mu\text{m}$  to examine the influence from viscous liquid damping. The sensor fabrication processes are shown in Fig. 4 and described as follows.

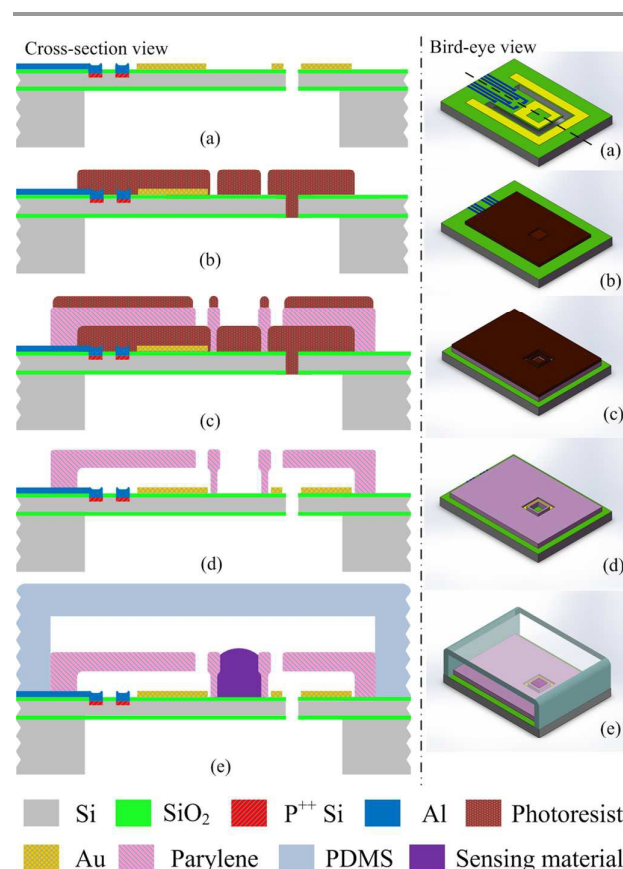


Fig. 4 Fabrication process steps of the liquid-phase resonant bio/chemical detection chip, with cross-sectional views at the left side and the corresponding 3D bird-eye views at right. (a) Formation of the integrated resonant cantilever. (b) Thick photoresist is patterned as sacrificial layer. (c) Parylene thin-film deposition and patterning. (d) Air-gap and sensing-pool release to free the resonant sensor. (e) Embedding the sensor into a micro-fluidic chip for bio/chemical detection.

(a): The silicon micro-cantilevers are fabricated in (100) silicon-on-insulator (SOI) water, with the electro-thermal resonance-exciting and piezo-resistive signal-reading elements integrated. The detailed process steps can be referred to our previous literature of Ref. 38. It is worthy pointing out that the gap distance between the edge of the cantilever and the structure frame should be less than 6  $\mu\text{m}$ . The purpose is to prevent the following coated photoresist from flowing into the groove. Au film is sputtered and patterned around the 'sensing-pool' and the region under the narrow slit, which is hydrophobic and is helpful for resisting against water-vapour condensation onto the  $\text{SiO}_2$  surface of the cantilever.

(b): Thick photoresist is spray-coated and patterned as sacrificial-layer. The thickness of the photoresist determines the gap-size  $G$  between the parylene-film and the resonant cantilever.

(c): A hydrophobic parylene cover-layer of 6  $\mu\text{m}$  in thickness is chemically deposited and patterned with oxygen plasma etching. Another photoresist layer is used as the mask for the oxygen plasma etching, where the etching ratio between photoresist and parylene is about 1:1.3.

(d): In 60°C water bath, the resonator is freed by removing the sacrificial-layer with Baker PRS-3000™ photoresist stripper.

(e): After specific sensing-material is loaded into the 'sensing-pool' of the cantilever, PDMS made micro-chamber and micro-channels are constructed, in which the resonant cantilever is embedded. The formed LOC sensing system can be referred to the schematic structure sketched in Fig. 1a.

#### Sensing-material preparation and loading into the sensing-pool

We design two kinds of sensing materials for real-time liquid-phase detection to chemical and biological substances, respectively. One material is a hyper-branched polymers (HBP), which is functionalized with the sensing group of 2,2-Bis(4-hydroxyphenyl)-hexafluoropropane (BHPF) for detection of trace-concentration residual pesticide of acephate in aqueous solution. The other one is anti-*E. coli* DH5 $\alpha$  polyclonal antibody (pAb) for detection of *E. coli* DH5 $\alpha$  in PBS.

For specific adsorption of acephate molecules, we synthesize the sensing material at first and, then, load it onto the resonant micro-structure. Preparation of the hydrogen-bond functionalized acidic HBP includes synthesis of HBP and modification with BHPF sensing-group tailed compound. The detailed information can be referred to Ref. 39. After preparation of the sensing material, 10 mg BHPF functionalized HBP is dissolved in 1 mL tetrahydrofuran (THF) to form clear solution. Then the aqueous sample is loaded into the sensing pool on the resonant cantilever, by using a commercial micro-manipulator (Eppendorf PatchMan NP2). The loading process is aided by inspection under a microscope (Leica DM4000). After that, the resonant micro-sensor is dried in an oven at 45°C for about 2 hrs. Then it is covered with the previously made PDMS micro-channel chip to form the liquid-phase detection micro-system.

In order to make the resonant sensing micro-chip for liquid-phase bacteria detection, we immobilize the anti-*E. coli* DH5 $\alpha$

pAb into the sensing-pool of the resonant micro-cantilever through a layer-by-layer self-assembly route. The biotinylated anti-*E. coli* DH5 $\alpha$  pAb sample is purchased from Pierce Rockford. Bovine serum albumin (BSA), glutaraldehyde, 3-aminopropyltriethoxysilane (APTES) and streptavidin are purchased from Sigma-Aldrich. The sample of *E. coli* is cultured in our own laboratory. The layer-by-layer immobilization is initiated from the  $\text{SiO}_2$  sensing-pool surface of the cantilever. In a Harrick Plasma Cleaner PDC-32G, the surface of the resonant cantilever is cleaned with oxygen plasma for 45 sec (under 18 W power). Then the sensing-pool is silanized in a chamber with 50  $\mu\text{L}$  APTES at 80°C. After the gas-phase self-assembly of APTES for 2 hrs, the sensor is annealed at 80°C for 1 hr. Thereafter, 2.5% glutaraldehyde in PBS (pH=7.5) is added to the silanized amine  $\text{SiO}_2$  surface to react for 1 hr. After eluted with PBS, the sensing structure is incubated with 1 mg/mL streptavidin in PBS (at 4°C) for 12 hrs. The streptavidin functionalized surface is washed with PBS for several times and, then, coated with 1% BSA for blocking the non-specific sites. 0.3 mg/mL sample of biotinylated pAb (prepared in 1% BSA) is introduced for 1 hr to complete the antibody immobilization. Finally, the pAb functionalized cantilever is covered with the PDMS micro-channel chip for online biological detection.

#### Experimental setup

After the sensing-material loaded, the resonant sensor is sealed into a PDMS made micro-channel system which allows the inlet and outlet to link with polytetrafluoroethylene (PTFE) tubes, as is schematically shown in Fig. 1a. With a peristaltic pump, liquid can be driven in and out with a controllable speed. Aided by a lab-made phase-locked-loop (PLL) interface circuit, the frequency-shift detection signal from the resonant cantilever is real-time read out with a digital frequency counter (Agilent 53131A) and recorded in a personal computer.

## Results and discussion

#### SEM characterization

Fig. 5a shows the SEM image of the fabricated resonant cantilever that is dressed in the parylene-made  $\mu\text{-}$ 'diving suit'. The close-up view of the sensing-pool is shown in Fig. 5b, in which the locally loaded HBP sensing-material can be seen clearly. In order to look into the  $\mu\text{-}$ 'diving suit', the parylene film on top of the cantilever is striped off by using oxygen plasma ashing process, and the previously buried resonant cantilever is exposed and shown in the SEM image of Fig. 5c. To view the sacrificial-layer released air gap between the parylene-film and the silicon-cantilever at beneath, the  $\mu\text{-}$ 'diving suit' together with the cantilever is partly cut by using a focused-ion-beam (FIB) machine (FEI Quanta 3D FEG 600), with the detailed structure at the sensing-pool location and its further magnification view shown in Figs. 5d and Fig. 5e, respectively. The about 8  $\mu\text{m}$  air gap between parylene and cantilever can be seen clearly.

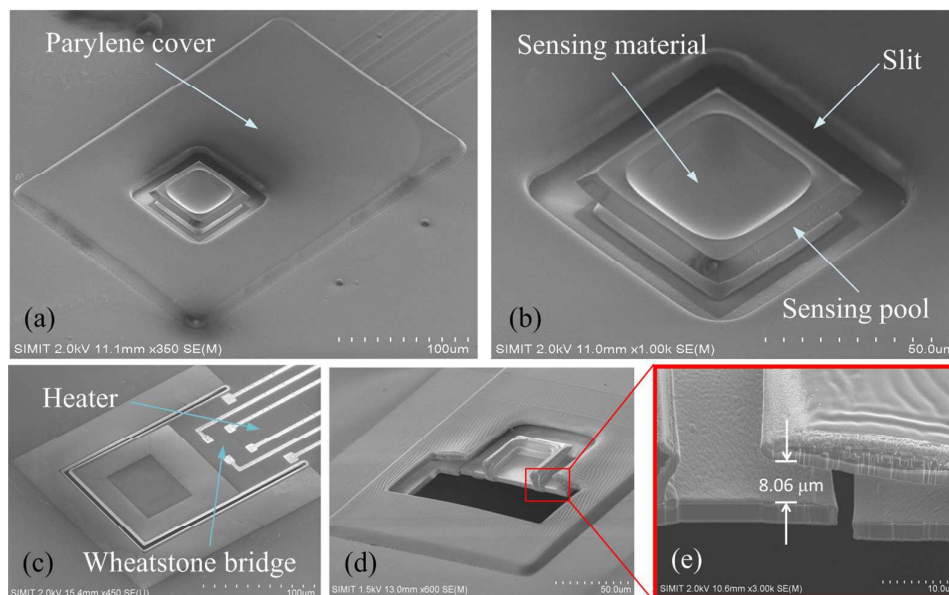


Fig. 5 (a) SEM image of the fabricated resonant cantilever sensor that is dressed in the  $\mu$ -'diving suit' for water-proof but with a sensing-pool area to contact liquid analyte. (b) Close-up view of the sensing-material loaded sensing-pool and the surrounding narrow slit that is made of hydrophobic parylene. (c) After the parylene  $\mu$ -'diving suit' is peeled off, the integrated resonant cantilever is exposed. (d): With the sensing-pool structure partly cut by FIB, the parylene-made water-proof slit structure can be seen, with the magnified view showing the air gap between the parylene film and the cantilever.

### Q-factor of the resonant sensor

After the  $\mu$ -'diving suit' dressed resonant micro-cantilever is embedded in the fluidic channel, as is shown in Fig. 6a, the resonance characteristics in both air and deionized (DI) water are tested by using an Agilent-E5072A network analyzer. Fig. 6b shows the measured amplitude-frequency curve of a resonant sensor, which has  $70\ \mu\text{m} \times 70\ \mu\text{m}$  opening size and  $12\ \mu\text{m}$  air gap. In ambient air the resonant frequency of the sensor is  $102.275\ \text{kHz}$  while the  $Q$ -factor is 65. After the channel is filled with water, the resonant frequency and the  $Q$ -factor both drop to  $50.615\ \text{kHz}$  and 23, respectively. The decrease in resonant frequency is mainly due to the equivalent additional mass of the liquid. Thanks to the  $\mu$ -'diving suit' technique, the decrease in the open-looped  $Q$ -factor is acceptable that is originated from the heavier liquid damping effect on the exposed sensing-pool area. As is explicated in previous section of the paper, different resonant structures with different gaps and opening sizes will exhibit different  $Q$ -

factors. In air and in water, respectively, we have measured the resonant frequencies and  $Q$ -factors of the sensors with different structure parameters. The testing results support following conclusions. No matter in air or in water, the resonant micro-sensor with  $12\ \mu\text{m}$  gap always has higher  $Q$ -factor than that with  $8\ \mu\text{m}$  gap. Moreover, larger opening size (i.e. sensing-pool area) brings about higher  $Q$ -factor only in air. In water however, the resonant sensor with smaller opening size achieves higher  $Q$ -factor. This is because larger opening means larger contact area with water and larger energy dissipation. For comparison, we peel off the parylene film by oxygen plasma etching and test the  $Q$ -factor of the cantilever without the  $\mu$ -'diving suit'. In air, the tested  $Q$  value is 182. In water however, the  $Q$ -factor becomes too low to be measured. All the tested open-loop  $Q$  values of the cantilevers are compared together in Table 1. Although even smaller opening area helps to obtain higher  $Q$ -factor, we do not choose such devices, for the sensing-pool size should be large enough for capturing enough number of molecules, i.e. adsorbing enough mass, to realize rapid micro-gravimetric detection. Moreover, the sensing-pool size needs to be large enough when the big-sized bio-substances are detected, such as bacteria or cells.

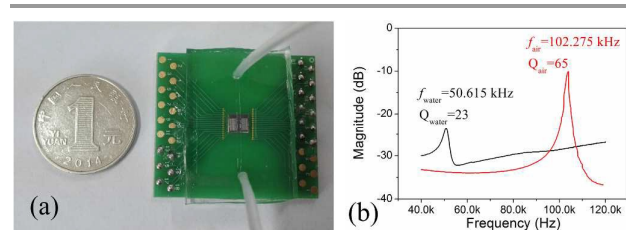


Fig. 6 (a) Photograph of the resonant-cantilever embedded liquid bio/chemical detection micro-system. (b) Tested amplitude-frequency characteristics of the resonant sensor in air (in red curve) and in water (in black curve), including the resonant frequencies and the  $Q$ -factors.

Table 1 Tested resonance  $Q$ -factor versus gap-size and opening-size on the parylene film.

$Q$ -factor in air/in water		Opening size on the parylene film	
		$70 \times 70\ \mu\text{m}$	$100 \times 75\ \mu\text{m}$
Air gap	$8\ \mu\text{m}$	37/14	58/10
	$12\ \mu\text{m}$	65/23	93/17
After parylene peeled from a cantilever with $70 \times 70\ \mu\text{m}$ opening size and $12\ \mu\text{m}$ gap		182/NA	

Therefore, we finally choose the resonant micro-sensors with the gap distance as 12  $\mu\text{m}$  and the opening size as 70  $\mu\text{m}$   $\times$  70  $\mu\text{m}$  for subsequent bio/chemical sensing experiments.

#### Assessment of continuous working period in liquid

As is pointed out in the earlier section, three aspects are employed in structure design to extend liquid-phase working time of the resonant sensor. Firstly, the narrow slit constructed by hydrophobic parylene can effectively reject liquid leakage. Secondly, the patterned hydrophobic Au film under the opening can depress water vapour condensation. Thirdly, to further absorb water vapour that diffuses and slowly accumulate under the  $\mu$ -'diving suit' that limits the continuous working period of the liquid-phase sensing system, we put moisture absorbing material from the wafer backside (i.e. under the cantilever). For assessment of the liquid-phase continuous working period of the sensor, we constantly monitor the resonant frequency signal of the cantilever resonance in water until the output signal changes sharply and, simultaneously, the noise increases significantly. The monitored phenomena indicate water leakage through the slit. For comparison, we test two types of resonant sensors with one has wide gap ( $t=25\ \mu\text{m}$ ) and another has the optimally designed narrow slit ( $t=10\ \mu\text{m}$ ). The corresponding test results are shown in Figs. 7a and 7b. For the wide gap resonant sensor, normal resonance period under water-proof condition is generally less than 7 hours, after which the frequency firstly decreases sharply and then cannot be measured due to the much lowered  $Q$ -factor. After the liquid front enters from the wide gap, it will gradually flows into the 12  $\mu\text{m}$  thick air gap where the parylene/gold walls cannot reject the water flow for too long a period. In contrast, the resonant sensors with the narrow slit design can always keep the water-proof resonance for longer than 20 hours. To further evaluate the anti-leakage function of the  $\mu$ -'diving suit' in complex bio-solutions, we test the resonating behaviour of the sensors with the narrow slit in two typical bio-solutions of PBS-2% BSA and RPMI-1640 cell culture medium (Gibco). According to the experimental results shown in Fig. 7b, the sensors can also stably resonate in the high-concentration or complex biological solutions for longer than 20 hours. Within the long working time of about one day, most of bio/chemical detection and online analysis processes can be well completed.

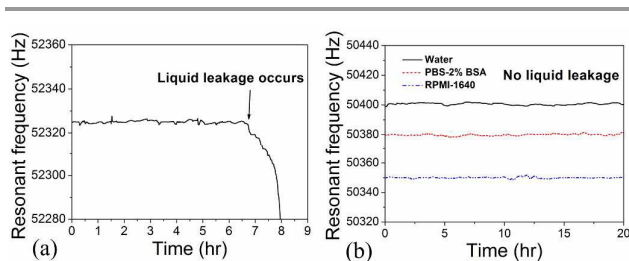


Fig. 7 Tested resonant frequency versus continuous resonating period of time in solutions: (a) for the structure with a wide gap around the sensing-pool in water; (b) for the structure with a narrow slit around the sensing-pool in three types of solutions.

#### Real-time bio/chemical sensing

In the resonant cantilever embedded microfluidic chip, liquid samples can flow through the cantilever and goes out via the outlet with controllable flow rate. After the flow rate becomes stable, we start to record the resonant frequency of the sensor. In the experiment of acephate detection, 10 mL DI water flows in the close-looped fluidic channel, as is shown in the schematic setup of Fig. 8a. Continually driven by a market available peristaltic pump, the water flow circulates in the closed loop. After the frequency base-line is recorded for a few minutes, 10  $\mu\text{L}$  of acephate solution with 100 ppm volume concentration is injected and mixed into the water fluid so that the concentration of the aqueous acephate is rapidly diluted down to 100 ppb. As is shown in Fig. 8b, the recorded resonant frequency of the acephate sensor (in black solid line) begins to decrease due to mass adsorption of organo-phosphorous molecules that are specifically captured by the BHPF-groups of the functionalized sensing-material. The frequency-shift gets saturated within three minutes and the sensing signal of about 50 Hz is obtained. A few minutes is needed for re-stability of the resonant frequency. Then, the second 10  $\mu\text{L}$  acephate solution with volume concentration of 100 ppm is injected again and a further frequency-shift signal is observed. At this time, the concentration of the acephate solution has been changed to 200 ppb. By repeating such a way to change the concentration of the acephate solution sequentially to 300 ppb and 400 ppb, the frequency-shift sensing signals in Fig. 8b clearly exhibits the corresponding stepped decreases of the sensor. At last, the close-loop is opened and DI water is introduced to replace the entire fluid. Then the resonant frequency recovers to the value near the original base-line. Control experiment is carried out. Under the same conditions, the sensing signal of a sensor for control experiment (i.e., without sensing material loaded) is recorded in Fig. 8b with the red dash-line, where no obvious sensor response can be

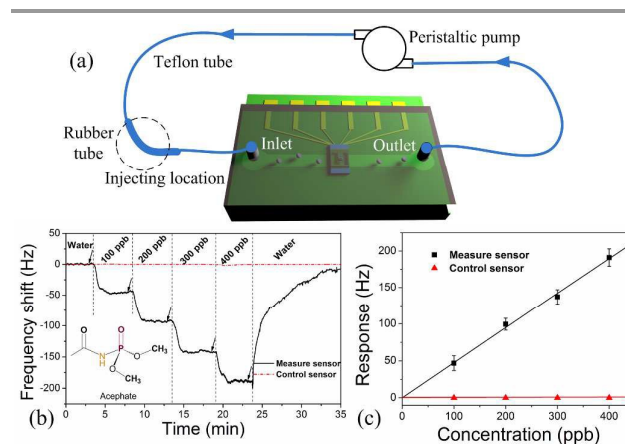


Fig. 8 (a) Schematic diagram of the close-looped fluidic system. (b) Frequency responses of the acephate sensor (in black solid line) and the sensor for control experiment (in red dashed line) versus concentration of aqueous pesticide of acephate. The concentration is stepwise increased from 100 ppb to 400 ppb, with 100 ppb as the increment. The arrows indicate the moments when the sample is injected to the fluid. (c) Responses of the acephate sensor (in black squares) and the sensor for control experiment (in red triangles) to the acephate solutions with various concentrations.

observed. In addition, when 10  $\mu\text{L}$  of DI water instead of the acephate solution is injected into the fluid, no obvious sensor response can be observed either. Our experiment also shows that, the frequency base-line can be influenced by sufficient change of liquid viscosity. Fig. 8c shows the experimentally obtained relationship between the sensor response and the concentration of the acephate solution. For each concentration the test is repeated for five times to obtain the averaged response. The experimentally obtained sensitivity is about 50Hz per 100ppb, and the noise-floor of the frequency signal is about 5Hz. Based on the generally accepted criterion that the minimum detectable signal should be 3 times of the noise-floor (i.e., S/N ratio=3), the LOD of the sensor to aqueous acephate is estimated as dozens of ppb.

As for detection of *E. coli* DH5 $\alpha$ , firstly we use PBS instead of DI water to fill into the micro-channel to stabilize the signal baseline. With a certain concentration, the sample of *E. coli* DH5 $\alpha$  in PBS is introduced to the sensor and the generated frequency-shift signal is recorded in Fig. 9. Fig. 9a shows the frequency responses of a series of bacteria sensors to serial concentrations of *E. coli* DH5 $\alpha$  in PBS (from  $10^2$  CFU/mL to  $10^5$  CFU/mL). The sample with higher concentration generates larger frequency-shift signal but needs longer response time. The sensors are selected from the same fabrication and antibody immobilization batch, thereby featuring very close mass sensitivity. By using the experimental method described in Ref. 40, the mass sensitivity is calibrated by loading micro-beads (with known mass) in the sensing-pool of the cantilever. In Fig. 9b, the sensing response versus concentration of the bacteria is plotted, and the corresponding results for control experiment (by using the sensors without the antibody immobilized) are recorded together for comparison. The data in Fig. 9b are the averaged results for three-time detection, with the error bars denoted. It can be seen from Fig. 9 that the minimum detectable concentration is about 100 CFU/mL. The inset SEM image in Fig. 9b shows the *E. coli* DH5 $\alpha$  bacteria adsorbed on the sensor via specific binding with the antibody.

## Conclusions

We have proposed and developed a new technology to ensure micro-cantilever sensor long-time resonating in solution for

real-time bio/chemical detection and real-time analysis. With a  $\mu$ -'diving suit' design, a hundreds of microns sized resonant cantilever, with electro-thermal driving and piezoresistive frequency readout on-cantilever integrated, is embedded into a fluidic micro-chip. The micro-gravimetric sensor experimentally exhibits long-time (at least 20 hours) continuous resonance in solution and the  $Q$ -factor in water achieve as high as 23. Loaded with the specific sensing-materials to acephate pesticide of fluorinated phenol modified hyper-branch polymer, sensing experiments has resulted in rapid detection of residual acephate solution of 100 ppb to 400ppb. When the sensing material is change to anti-*E. coli* DH5 $\alpha$  pAb, the resonant bio-sensing micro-systems successfully detect *E. coli* DH5 $\alpha$  (in PBS) with a series of concentrations. This novel technical method is promising widely in various liquid-phase bio/chemical detections by using micro-mechanical resonant sensing structures.

## Acknowledgements

This research is supported by NSF of China (91323304, 61571430, 61321492, 31200056, 61401446) and Science and Technology Commission of Shanghai (14521106100).

## References

- L. Nan, Z. D. Jiang and X. Y. Wei, *Lab Chip*, 2014, **14**, 1060-1073.
- B. Schwarz, P. Reininger, D. Ristanic, H. Detz, A. M. Andrews, W. Schrenk and G. Strasser, *Nat. Commun.*, 2014, **5**, 4085.
- P. Neuzil, C. D. M. Campos, C. C. Wong, J. B. W. Soon, J. Reboud and A. Manz, *Lab Chip*, 2014, **14**, 2168-2176.
- S. Bouguelia, Y. Roupioz, S. Slimani, L. Mondani, M. G. Casabona, C. Durmort, T. Vernet, R. Calemczuk and T. Livache, *Lab Chip*, 2013, **13**, 4024-4032.
- R. Lee, I. Jung, M. Park, H. Ha and K. H. Yoo, *Lab Chip*, 2013, **13**, 3410-3416.
- J. Zhang, S. Liu, P. Yang and G. Sui, *Lab Chip*, 2011, **11**, 3516-3522.
- J. Lee, M. Jo, T. H. Kim, J. Y. Ahn, D. K. Lee, S. Kim and S. Hong, *Lab Chip*, 2011, **11**, 52-56.
- V. Velusamy, K. Arshak, O. Korostynska, K. Oliwa and C. Adley, *Biotechnol. Adv.*, 2010, **28**, 232-254.
- T. Fukuba, Y. Aoki, N. Fukuzawa, T. Yamamoto, M. Kyoe and T. Fujii, *Lab Chip*, 2011, **11**, 3508-3515.
- X. Huang, C. Leduc, Y. Ravussin, S. Q. Li, E. Davis, B. Song, D. C. Li, K. X. Xu, D. Accili, Q. Wang, R. Leibel, Q. Lin, *Lab Chip*, 2014, **14**, 294-301.
- T. Thundat, E. A. Wachter, S. L. Sharp and R. J. Warmack, *Appl. Phys. Lett.*, 1995, **66**, 1695-1697.
- P. C. Xu, X. X. Li, H. T. Yu and T. G. Xu, *Sensors*, 2014, **14**, 19023-19056.
- J. Tamayo, P. M. Kosaka, J. J. Ruz, Á. S. Paulo and M. Calleja, *Chem. Soc. Rev.*, 2013, **42**, 1287.
- B. N. Johnson and R. Mutharasan, *Biosens. Bioelectron.*, 2012, **32**, 1-18.
- A. Boisen, S. Dohn, S. S. Keller, S. Schmid and M. Tenje, *Rep. Prog. Phys.*, 2011, **74**, 036101.
- H. T. Yu, P. C. Xu, X. Y. Xia, D.-W. Lee and X. X. Li, *IEEE Trans. Ind. Electron.*, 2012, **59**, 4881-4887.
- H. T. Yu, P. C. Xu, D.-W. Lee and X. X. Li, *J. Mater. Chem. A*, 2013, **1**, 4444-4450.

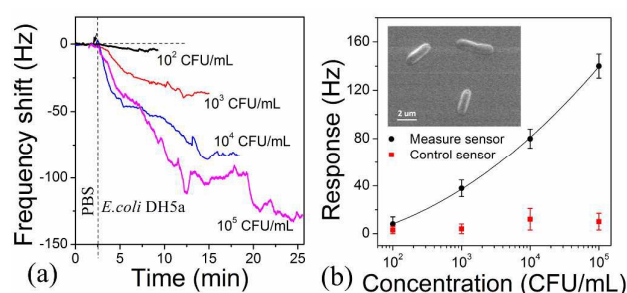


Fig. 9 (a) Frequency signals of the bacteria sensors to serial concentrations of *E. coli* DH5 $\alpha$  in PBS. (b) Relationship between the sensing response and concentration of *E. coli* DH5 $\alpha$  in PBS. The control experiment results are also shown together for comparison.

- 18 H. T. Yu, T. T. Yang, Y. Chen, P. C. Xu, D. -W. Lee and X. X. Li, *Anal. Chem.*, 2012, **84**, 6679-6685.
- 19 P. C. Xu, H. T. Yu and X. X. Li, *Anal. Chem.*, 2011, **83**, 3448-3454.
- 20 N. V. Lavrik, M. J. Sepaniak and P. G. Datskos, *Rev. Sci. Instrum.*, 2004, **75**, 2229-2253.
- 21 K. M. Goeders, J. S. Colton and L. A. Bottomley, *Chem. Rev.*, 2008, **108**, 522-542.
- 22 W. B. Zhang and K. Turner, *Sens. Actuators, A*, 2007, **134**, 594-599.
- 23 A. P. Davila, J. Jang, A. K. Gupta, T. Walter, A. Aronson and R. Bashir, *Biosens. Bioelectron.*, 2007, **22**, 3028-3035.
- 24 C. Vančura, Y. Li, J. Lichtenberg, K.-U. Kirstein and A. Hierlemann, *Anal. Chem.*, 2007, **79**, 1646-1654.
- 25 Y. H. Tao, X. X. Li, T. G. Xu, H. T. Yu, P. C. Xu, B. Xiong and C. Z. Wei, *Sens. Actuators, B*, 2011, **157**, 606-614.
- 26 T. Burg, M. Godin, S. Knudsen, W. Shen, G. Carlson, J. Foster, K. Babcock and S. Manalis, *Nature*, 2007, **446**, 1066-1069.
- 27 J. Park, S. Nishida, P. Lambert, H. Kawakatsu and H. Fujita, *Lab Chip*, 2011, **11**, 4187-4193.
- 28 H. T. Yu and X. X. Li, *Appl. Phys. Lett.*, 2009, **94**, 011901.
- 29 A. B. D. Cassie and S. Baxter, *Trans. Faraday Soc.*, 1944, **40**, 546.
- 30 R. N. Wenzel, *Ind. Eng. Chem.*, 1936, **28**, 988-994.
- 31 T. Wu and Y. Suzuki, *Sens. Actuators, B*, 2011, **156**, 401-409.
- 32 C. P. Green and J. E. Sader, *J. Appl. Phys.*, 2005, **98**, 114913.
- 33 M. Bao and H. Yang, *Sens. Actuators, A*, 2007, **136**, 3-27.
- 34 T. Veijola, *J. Micromech. Microeng.*, 2004, **14**, 1109.
- 35 C. R. Doering, *Annu. Rev. Fluid Mech.*, 2009, **41**, 109-128.
- 36 M. H. Bao, H. Yang, H. Yin, Y. C. Sun, *J. Micromech. Microeng.*, 2002, **12**, 341-346.
- 37 C. Vančura, I. Dufour, S. M. Heinrich, F. Josse and A. Hierlemann, *Sens. Actuators, A*, 2008, **141**, 43-51.
- 38 H. T. Yu, X. X. Li, X. H. Gan, Y. J. Liu, X. Liu, P. C. Xu, J. G. Li and M. Liu, *J. Micromech. Microeng.*, 2009, **19**, 045023.
- 39 C. Hartmann-Thompson, J. Hu, S. N. Kaganove, S. E. Keinath, D. L. Keeley and P. R. Dvornic, *Chem. Mater.*, 2004, **25**, 5357-5364.
- 40 T. G. Xu, H. T. Yu, P. C. Xu and X. X. Li, *Biomed. Microdevices*, 2012, **14**, 303-311.